Viscoelastic Dynamics of Actin Filaments Coupled to Rotary F-ATPase: Curvature as an Indicator of the Torque

Dmitry A. Cherepanov and Wolfgang Junge
Division of Biophysics, University of Osnabrück, D-49069 Osnabrück, Germany

ABSTRACT ATP synthase (F-ATPase) operates as an electrochemical-to-mechanical-to-chemical energy transducer with an astounding 360° rotary motion of subunits $\epsilon\gamma\mathbf{c}_{10-14}$ (rotor) against $\delta(\alpha\beta)_3\mathbf{ab}_2$ (stator). The enzyme's torque as a function of the angular reaction coordinate in relation to ATP-synthesis/hydrolysis, internal elasticity, and external load has remained an important issue. Fluorescent actin filaments of micrometer length have been used to detect the rotation as driven by ATP hydrolysis. We evaluated the viscoelastic dynamics of actin filaments under the influence of enzyme-generated torque, stochastic Langevin force, and viscous drag. Modeling with realistic parameters revealed the dominance of the lowest normal mode. Because of its slow relaxation (~100 ms), power strokes of the enzyme were expected to appear strongly damped in recordings of the angular velocity of the filament. This article describes the theoretical background for the alternative use of the filament as a spring balance. The enzyme's angular torque profile under load can be gauged by measuring the average curvature and the stochastic fluctuations of actin filaments. Pertinent experiments were analyzed in the companion paper.

INTRODUCTION

ATP synthase generates ATP in F_1, its peripheral portion, at the expense of proton flow through F_O, its membrane portion. The enzyme operates as two rotary motors. They are coupled by a central shaft and hold together by an eccentric bearing (for reviews see Junge et al., 1997; Boyer, 1997; Kinosita et al., 1998; Oster and Wang, 1999; Leslie et al., 1999)). The "rotor" elements, subunits $\epsilon\gamma\mathbf{c}_{10-14}$, move relative to the "stator" elements, subunits $\mathbf{ab}_2\delta(\alpha\beta)_3$. Depending on the dominant driving force, be it ion-motive or chemical, one motor runs forward as a motor and the other one backward as a generator. Both motor/generators are evidently rotary steppers, with C_3 symmetry in F_1 (Abrahams et al., 1994) (but see also Sabbert and Junge, 1997; Yasuda et al., 1998), and a still-debated C_{10}-, C_{12}-, or C_{14} symmetry in F_O (Jones and Fillingame, 1998; Stock et al., 1999; Seelert et al., 2000). An elastic power transmission has been claimed to cope with the symmetry mismatch (Cherepanov et al., 1999; Pänke and Rumberg, 1999).

With its well-separated partial functions—electrochemical, mechanical, and chemical—this twin-engine is an excellent object for studies on nanomechanics. The ultimate goal is to understand the functioning of this astounding machine at the molecular scale. The relative rotation of subunits in the isolated F_1 portion has been detected by chemical cross-linking (Duncan et al., 1995), polarized absorption recovery after photobleaching (Sabbert et al., 1996) and, most spectacularly, by microvideography using fluorescent actin filaments that were attached to the rotor portion of immobilized single F_1-molecules (Noji et al., 1997). This technique has recently been expanded to F_OF_1 constructs (Sambongi et al., 1999; Tsunoda et al., 2000; Pänke et al., 2000). The average torque that is generated by ATP hydrolysis, ~40 pN/nm (Yasuda et al., 1998) has been calculated from the average rotation rate of the actin filaments under the debatable assumption that the rotation was controlled by the viscous drag of bulk fluid rather than by surface contacts. If ATP hydrolysis occurred at unphysiologically low ATP concentration (10 nM), a three-stepped rotation was detected (Kinosita et al., 1998; Adachi et al., 2000). This stepping, however, reflects the diffusion-controlled supply of the next nucleotide rather than the dynamic behavior of the enzyme under normal conditions ([ATP] $\gg$ 10 μM). Under saturating ATP concentrations we obtained evidence for threefold stepping using a single dye molecule as a probe on subunit γ (Sabbert and Junge, 1997; Sabbert et al., 1997; Häsler et al., 1998). No such stepping has been detected using actin filaments. Apparently the viscous damping of the *long* actin filament in the liquid has obscured the rotary dynamics of the enzyme.

These considerations prompted us to scrutinize the viscoelastic mechanics of the enzyme–filament construct. This article outlines the theory. Following common practice in mechanics, the dynamic behavior of F-actin was described in terms of orthonormal modes. Because the viscous drag in the fluid is much greater than the small inertia of the filaments, the dynamics of filaments is over-damped, relaxing instead of oscillating. The spatial shapes of these modes resemble the familiar ones of an oscillating cantilever with n ($n = 0, 1, 2, 3, \ldots$) nodes over the length, excluding the ends. A simulation of the dynamic behavior of rotating actin filaments using realistic parameters showed that the fundamental normal mode with the longest relaxation time (100 ms) dominated the behavior in the time range of 10 ms, whereas higher modes were of negligible extent and rapidly

Received for publication 15 February 2001 and in final form 6 June 2001.

Address reprint requests to Dr. Wolfgang Junge, Dept. of Biology and Chemistry, University of Osnabruck, Barbarastrasse 11, D-49076 Osnabruck, Germany. Tel.: 49-541-969-2872; Fax: 49-541-969-2870; E-mail: junge@biologie.uni-osnabrueck.de.

D. A. Cherepanov's permanent address is Franklin Institute of Electrochemistry, Moscow, Russia.

0006-3495/01/09/1234/11 $2.00

damped away. As intuitively expected, the slow response of the lowest mode blurred fine details of the enzyme's internal rotary motion. However, the momentary curvature at the axis (see Eq. 3 below) was almost truly proportional to the torque at any given angular position. This was what was searched for and it has not been exploited until now.

The above considerations were based on an idealized situation, an actin filament driven at its fixed end by the rotary enzyme and moving in a homogeneous viscous fluid. In the realm of typical experiments, however, a filament of 3 μm length and $<$10 nm radius moves a few tens of nanometers over a rough surface of a protein-covered solid support. The viscosity close to the surface is not only greater than in the bulk (Hunt et al., 1994), but contacts with the surface may increase the apparent friction or even obstruct the motion. In an attempt to extend the validity of the above-described idealized concept we calculated the curvature of actin filaments at constant torque as a function of three different distributions of the compensating force over length. We found that the overall curvature was only slightly dependent on whether the force distribution was linear (viscous drag), constant (surface friction), or concentrated (obstacle contact). Broadly speaking, the idealized approach was applicable to typical experimental situations. In this article we present the theoretical background on the static curvature of actin cantilevers, their dynamic normal modes, the momentary curvature as a function of the transient torque generated by the enzyme, the transient elastic energy storage, and the analysis of thermal fluctuations. In the companion paper we evaluated data on fluctuating and rotating actin-cantilevers to yield 1) Young's modulus of elasticity of F-actin and 2) the torque profile of the chemical drive of F_OF_1 as a function of the angular reaction coordinate. Equations of crucial importance for the experimental companion paper are marked by underlined numbers in the following.

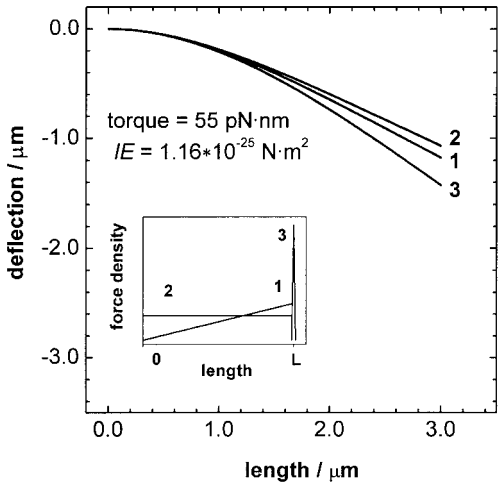

FIGURE 1 Static deformation of an elastic cantilever under three types of load distributions over its length (see *inset*). (1) Linearly increasing load as caused by a viscous drag on a rotating filament in a homogeneous fluid. (2) Uniformly distributed load (idealized friction at a solid surface). (3) Concentrated force acting on the very end of the cantilever (obstacle at the surface).

STATIC, DYNAMIC, AND STOCHASTIC DEFORMATIONS OF ACTIN FILAMENTS

Torque balance of rotating acting filaments

Fig. 1 in the companion paper (Pänke et al., 2001) illustrates the experimental situation. The enzyme is immobilized by His-tags on F_1 to a nickel-nitrilotriacetic acid-coated glass surface, head down and with the **c**-ring sticking out into the bulk solution. A fluorescent actin filament is attached to the **c**-ring by strep-tags. There was one engineered strep-tag on each of the identical subunits of the **c**-ring (Pänke et al., 2000). The filament, typically 2 μm long and with a diameter of 5.6 nm (Mendelson and Morris, 1997), moved $\sim$20 nm over a rough surface covered by horseradish peroxidase and ATP synthase. It is sufficient to approximate the filament by a cylindrical rod, and not necessary to consider its fine structure and the roughness of its surface, because the friction coefficient depends only weakly (logarithmically) on these properties.

It is evident that the torque generated by the rotary enzyme, $\boldsymbol{T}_0$, is counterbalanced by the torque that is attributable to 1) the inertia of the filament, $\boldsymbol{T}_I$; 2) the viscous drag, $\Gamma \cdot V$, (Γ denotes the corrected Stokes friction coefficient near the surface (Happel and Brenner, 1983), and $\boldsymbol{V}$ is the angular velocity); 3) the elastic and inelastic interactions with the surface, $\boldsymbol{T}_S$; and 4) the thermal Brownian fluctuations, $\boldsymbol{T}_B$. The torque balance then reads:

$$\boldsymbol{T}_0 = \boldsymbol{T}_I + \Gamma \cdot \boldsymbol{V} + \boldsymbol{T}_S + \boldsymbol{T}_B \qquad (1)$$

In the case of slowly rotating actin filaments, which is considered here, i.e., at very low Reynolds numbers, the inertial torque is smaller than the other components by several orders of magnitude, and it can be eliminated from consideration (Happel and Brenner, 1983; Berg, 1993). Additionally, the torque generated by Brownian motion averages to zero.

Static elastic deformation of a cantilever under constant torque

In this section we ignored thermal fluctuations (Langevin forces) and dynamic effects, and considered the static elastic deformation of the actin cantilever due to 1) the torque of the rotary enzyme acting on the "fixed" end of the cantilever, and 2) a compensating counter-torque caused by external force acting on the filament. We considered three different types of force distributions over the filament length ($0 < x < L$), namely linearly increasing, constant, and concentrated at its very end (see inset to Fig. 1 for an illustration). These force distributions correspond to viscous

drag (proportional to the linearly increasing velocity of a rotating filament), surface friction (ideally considered as independent of the velocity), and a surface obstacle at the very end of the filament (concentrated force), respectively. The respective deformations of the cantilever under these three rather different loads are depicted in Fig. 1. They were calculated as follows by using the linear theory of elasticity (Landau and Lifshitz, 1959). The analysis of nonlinear effects is presented in the Appendix.

The bending moment in the filament, $M(x)$, depends on the distribution of the external forces over the filament length, $W(x)$:

$$\frac{d^2M}{dx^2} = W(x) \tag{2}$$

At the same time, the bending moment is proportional to the curvature of the cantilever:

$$M(x) = \frac{EI}{r} = EI\frac{d^2y}{dx^2} \tag{3}$$

where r denotes the radius of curvature, $y = y(x)$ is the deviation from the unbent filament position (filament deformation), and EI denotes the flexural rigidity of the cantilever (E is Young's modulus of the actin filament and I is the cross-sectional moment of the cantilever; for a cylinder with radius R, the factor I equals to $\pi/4R^4$). As the bending moment at the rotation axis, $M(x = 0)$, is equal to the driving torque generated by the enzyme, $\boldsymbol{T}_0$, the curvature at the axis (the fixed end) is proportional to $\boldsymbol{T}_0$:

$$\boldsymbol{T}_0 = EI\left.\frac{d^2y}{dx^2}\right|_{x=0} \tag{4}$$

In a static situation, the driving torque is equal to the counteracting one as generated by a given force distribution over length, $w(x)$:

$$\boldsymbol{T}_0 = \int_0^L w(x)x\,dx. \tag{5}$$

The solution has to match the boundary conditions for an elastic cantilever:

$$y|_{x=0} = 0, \quad \left.\frac{\partial y}{\partial x}\right|_{x=0} = 0. \tag{6}$$

The deformation of the cantilever, $y(x)$, was calculated by integrating Eqs. 2 and 3 with the boundary conditions 4–6 for the three types of force distribution described above. The analytical expressions for $y_i(x)$, $y_{ii}(x)$, and $y_{iii}(x)$ are given below and the respective graphs are shown in Fig. 1.

Linearly increasing force density (force/unit length) $w_i(x) = 3L^{-3}T_0x$:

$$y_i(x) = \frac{T_0x^2}{40EIL^3}(20L^3 - 10L^2x + x^3) \tag{7}$$

Constant force density $w_{ii}(x) = 2L^{-2}T_0$:

$$y_{ii}(x) = \frac{T_0x^2}{12EIL^2}(6L^2 - 4Lx + x^2) \tag{8}$$

Concentrated force: $w_{iii}(x) = L^{-1}T_0 \cdot \delta(x - L)$

$$y_{iii}(x) = \frac{T_0x^2}{6EIL}(3L - x) \tag{9}$$

where $\delta(x - L)$ is the Dirac delta function, $\int f(x)\delta(x - L)dx = f(L)$, with the dimension of the reciprocal length.

As evident from Fig. 1, the respective deformations over the full length are not too different. The maximal deformations, $y_k(L)$, are related as 1:0.9:1.2. The curvatures at the fixed end are, of course, the same (because the same total torque, $\boldsymbol{T}_0$, has been assumed for calculating the deformations, see Eq. 4).

The resolution of microvideography is limited by the diffraction length of light (<500 nm). Thus, it is impractical to read out the filament's curvature close to the enzyme axis (say at 10 nm). This limiting curvature can only be extrapolated from longer distance. The important result of the above considerations on the static deformation is that the extrapolation of the curvature to the fixed end of the cantilever yields the enzyme's torque independently of whether the major counter-force is viscous drag, surface friction, or a surface obstacle.

So far, only the static deformation of a filament has been considered. It approximates a situation where the enzyme turnover is drastically slowed or even totally blocked by either type of load on the filament.

Viscoelastic dynamics of a rotating filament

Discrete power strokes generated by the rotary enzyme may rapidly accelerate the actin filament. Mass-related inertia is negligible and viscous damping dominates the dynamic behavior, as mentioned. We asked for the delay and the distortion of the filament's motion over its length relative to the forced motion at its "fixed" end. The stochastic Langevin force, which averages to zero, was again neglected.

We considered a rotating cantilever in a viscous medium (see above). The torque applied to its fixed end, $\boldsymbol{T}_0(\theta)$, was assumed to be a well-behaved function of the angular position of the rotor, θ. For simulation purposes we assumed a test-torque profile with three periods over one full turn of 360° plus smaller components with higher angular frequencies. The angular accelerations were expected to generate a nonuniform elastic deformation of the cantilever.

The full displacement, $d\xi$, of a small fragment of the filament, length dx, at the coordinate x is the superposition of the axis rotation angle, $d\theta$, and the transverse filament deformation, dy:

$$d\xi = x \cdot d\theta + dy \tag{10}$$

As the inertial forces are negligibly small, the viscous force acting on the element dx, $\Gamma_0(\partial\xi/\partial t)$, matches the elastic force due to filament deformation, $EI(\partial^4 y/\partial x^4)$:

$$\Gamma_0 \frac{\partial \xi}{\partial t} = -EI \frac{\partial^4 y}{\partial x^4} \tag{11}$$

Here Γ_0 is the viscous friction coefficient of a small element, dx, of the rod with full length L and radius R rotating around one end in a liquid with the dynamic viscosity η, $\Gamma_0 = 4\pi\eta(\ln L/2R - 0.447)^{-1}$ (Hunt et al., 1994), and EI is the flexural rigidity. The friction coefficient of the whole filaments is $\Gamma = \frac{1}{3}\Gamma_0 L^3$.

We assume that the polar angle of the engine, θ, is a smooth function of time, as well as the angular velocity and acceleration:

$$\theta = \theta(t), \quad \boldsymbol{V}(t) = \frac{d\theta}{dt}, \quad a(t) = \frac{d^2\theta}{dt^2}. \tag{12}$$

The filament motion is then determined by the following inhomogeneous partial differential equation:

$$\frac{\partial y}{\partial t} + x \cdot v(t) = -D \frac{\partial^4 y}{\partial x^4} \tag{13}$$

where $D = EI/\Gamma_0$. The solution has to match the four boundary conditions: at the rotation axis ($x = 0$) two of them are given by Eq. 6, and at the free end ($x = L$) two other conditions read:

$$\left.\frac{\partial^2 y}{\partial x^2}\right|_{x=L} = 0, \quad \left.\frac{\partial^3 y}{\partial x^3}\right|_{x=L} = 0 \tag{14}$$

The general solution of the respective *homogeneous* equation

$$\frac{\partial \tilde{y}}{\partial t} = -D \frac{\partial^4 \tilde{y}}{\partial x^4} \tag{15}$$

can be developed into a sum of the viscoelastic normal modes of the cantilever

$$\tilde{y}(x, t) = \sum_{n=0}^{\infty} c_n \tilde{y}_n(x) \exp(-k_n t), \tag{16}$$

where $c_n (n = 0, 1, \ldots)$ denotes a set of still arbitrary amplitudes. Equation 16 describes the passive motion of a cantilever in a viscous medium in the absence of externally applied torque as the superposition of n exponential decay processes with characteristic relaxation times $\tau_n = k_n^{-1}$. The spatial factors of the normal modes, $\tilde{y}_n(x)$ $(n = 0, 1, 2, \ldots)$, satisfying the boundary conditions 6 and 14, read (see, e.g., Beth, 1967):

$$\tilde{y}_n(x) = L \cdot [\cosh(\delta_n x/L) - \cos(\delta_n x/L) + \alpha_n(\sinh(\delta_n x/L) - \sin(\delta_n x/L))] \tag{17}$$

where δ_n is the nth root of the equation $\cos(\delta_n)\cosh(\delta_n) = -1$ and

$$\alpha_n = -\frac{\cosh(\delta_n) + \cos(\delta_n)}{\sinh(\delta_n) + \sin(\delta_n)}.$$

The first four values of δ_n are $\delta_0 = 1.875$, $\delta_1 = 4.694$, $\delta_2 = 7.855$, and $\delta_3 = 10.995$. The characteristic relaxation rates of the cantilever therefore are:

$$k_n = \frac{EI}{\Gamma_0} \cdot \left(\frac{\delta_n}{L}\right)^4 \tag{18}$$

The modes $\tilde{y}_n(x)$ in Eq. 17 are eigensolutions of the self-adjoint linear differential operator, $\partial^4/\partial x^4$, and form a complete basis of orthogonal functions (see, e.g., Courant and Hilbert, 1962) with the normalization $L^{-3} \cdot \int_0^L \tilde{y}_n \tilde{y}_{n'} dx = \delta_{nn'}$.

It is worth noting that the relaxation of a cantilever is *forty* times slower than the relaxation of an unconstrained beam of the same length! The viscoelastic relaxation of an unconstrained beam was previously analyzed by several authors (see, e.g., Gittes et al., 1993), and the following expression for the relaxation rates was obtained:

$$k_n = \frac{EI}{\Gamma_0} \cdot \left(\frac{\pi(n+3)}{2L}\right)^4, \quad (n = 0,1,2,\ldots).$$

The strong sensitivity to the boundary conditions originates due to the fourth-power dependence on the filament length.

So far, only a passive motion of filaments has been discussed (solutions to the homogeneous differential equation). Next, we consider the motion that was driven by the rotary enzyme as induced by the angular velocity $\boldsymbol{V}(t)$ at the fixed end of the filament.

Let $\bar{y}_0(x, t)$ be a solution of the *inhomogeneous* equation

$$x \cdot \boldsymbol{V}(t) = -D \frac{\partial^4 \bar{y}_0}{\partial x^4} \tag{19}$$

matching the boundary conditions 6 and 14. It can be found by sequential integration:

$$\bar{y}_0(x, t) = \boldsymbol{V}(t) \cdot \frac{L^3}{6D} \cdot x^2 \left[-1 + \frac{x}{2L} - \frac{1}{20}\left(\frac{x}{L}\right)^3\right] = \boldsymbol{V}(t) \cdot \Psi_0(x) \tag{20}$$

Not surprisingly, the time-independent factor in Eq. 20, $\Psi_0(x)$, describes the same elastic deformation as the function $y_i(x)$ in Eq. 7, the static solution for a cantilever exposed to a linearly increasing load $w_i(x)$ (viscous drag exerted on a rotating cantilever). It can be expressed as a series of the normal modes:

$$\Psi_0(x) = \sum_{n=0}^{\infty} b_n \tilde{y}_n(x), \quad b_n = L^{-3} \cdot \int_0^L \Psi_0(x) \tilde{y}_n(x) dx \tag{21}$$

so that

$$\bar{y}_0(x, t) = \sum_n b_n \tilde{y}_n(x) \cdot \boldsymbol{V}(t) \tag{22}$$

The complete solution of 13 is the sum of the homogeneous and the inhomogeneous solutions:

$$y(x, t) = \sum_{n=0}^{\infty} [b_n V(t) + c_n(t) \cdot \exp(-k_n t)] \cdot \tilde{y}_n(x)$$

$$\equiv \sum_{n=0}^{\infty} A_n(t) \cdot \tilde{y}_n(x) \tag{23}$$

Substituting this equation into 13 results in the ordinary differential equations for $c_n(t)$:

$$\frac{dc_n}{dt} = -b_n \cdot a(t) \cdot \exp(k_n t)$$

where $a(t)$ is the angular acceleration. The solution gives the coefficients $A_n(t)$:

$$A_n(t) = b_n \left[\boldsymbol{V}(t) - \int_0^t a(\tau) \exp(k_n(\tau - t)) d\tau - c_n(0) \right] \tag{24}$$

where the coefficients $c_n(0)$ are determined by the initial state of the filament. It is evident that the contribution $A_n(t)$ of the normal mode n is proportional to the velocity $\boldsymbol{V}(t)$ if the respective relaxation rate k_n is higher than the characteristic frequency of the angular acceleration $a(t)$.

The torque $\boldsymbol{T}$ generated by the engine is a function of the angular position of the filament, θ, at the rotation axis, $\boldsymbol{T} = \boldsymbol{T}(\theta)$. This torque is equal to the momentary bending moment of the filament at $x = 0$ (see Eq. 4). If the rotation is periodical, the initial values $c_n(0)$ can be set to zero. From Eq. 4 one finds

$$\boldsymbol{T}(\theta) = -EI \left. \frac{\partial^2 y}{\partial x^2} \right|_{x=0}$$

$$= -\frac{2EI}{L} \int_0^t \frac{\partial^2 \theta}{\partial \tau^2} \sum_n b_n \delta_n^2 [1 - \exp(k_n(\tau - t))] d\tau \tag{25}$$

If the time-dependence of the forced angular motion, $\theta(t)$, is known, expression 24 is the exact solution of the problem and one finds the torque as function of the angle by solving Eq. 25. The original task of the experimentalist, however, is the opposite; namely, to find the dynamics of the driving motor, $\theta(t)$, based on experimental data on the angular dependence of the torque, $\boldsymbol{T}(\theta)$. This requires a solution of the integro-differential Eq. 25.

An analytical solution is readily obtained if the contribution of the lowest normal mode is much larger than the contributions of the rest: $|A_0(t)| \gg |A_1(t)|, |A_2(t)|, \ldots$. Then Eq. 25 simplifies:

$$\int_0^t \frac{\partial^2 \theta}{\partial \tau^2} [\exp(k_0 t) - \exp(k_0 \tau)] d\tau = \frac{\boldsymbol{T}(\theta) L \exp(k_0 t)}{2EI b_0 \delta_0^2} \tag{26}$$

By differentiation one finds the first-order ordinary differential equation

$$\frac{d\theta}{dt} = \frac{-k_0 T(\theta)}{2EI k_0 b_0 L^{-1} \delta_0^2 + \dfrac{\partial T(\theta)}{\partial \theta}} \tag{27}$$

which connects the unknown angular evolution $\theta(t)$ with the experimentally accessible angular torque as a function of the angle $\boldsymbol{T}(\theta)$.

Figs. 2 and 3 illustrate a representative example of filament dynamics. The rotation is forced by the enzyme's torque, $\boldsymbol{T}(\theta)$. Let us take as an example the function of the angular coordinate, which is plotted in Fig. 2 *A*. We used an arbitrary but realistic test function with three periods of torque (power strokes) over a full turn of 360°, and a time period of 2 s for one full revolution. High-frequency components of smaller magnitude were superimposed to the ground period. Fig. 2 *B* shows the assumed time course of the angular progression $\theta(t)$ in revolutions and of the momentary angular velocity $\boldsymbol{V}(t)$ in radians per second calculated numerically by solving Eq. 25 (*solid lines*), and the approximate solutions obtained by consideration of only the lowest normal mode by solving Eq. 27 (*broken lines*). The exact and the approximate solutions coincided very well; $\theta(t)$ and $\boldsymbol{V}(t)$ are periodical functions with the period of 667 ms or three periods over a full revolution, shaped after the three reactive sites in F_1. Whereas the angular progression revealed a moderately stepped behavior, the angular velocity displayed more dramatic oscillations.

The time-dependence of the extent of the first mode, $A_0(t)$, is depicted by the solid line in Fig. 2 *C*. The dashed and thin lines in Fig. 2 *C* show the next normal modes of the actin filament (their extent was scaled up by factors of 50 and 1000, respectively).

We conclude that the relative contributions of higher modes in the series of Eq. 21 are negligible. The respective amplitudes are proportional to the coefficients $b_0 = 1$, $b_1 = 4 \cdot 10^{-3}$, $b_2 = 2 \cdot 10^{-4}$, $b_3 = 10^{-5}$. Typical parameters of actin filaments in aqueous buffer were assumed as follows: $L \approx 3 \cdot 10^{-6}$ m, $R = 2.8 \cdot 10^{-9}$ m, $EI = 10^{-25}$ N · m^2 (Gittes et al., 1993; Yasuda et al., 1996), so that the respective relaxation rate constants are: $k_0 = 7\ s^{-1}$, $k_1 = 270\ s^{-1}$, $k_2 = 2100\ s^{-1}$, $k_3 = 8 \cdot 10^3\ s^{-1}$.

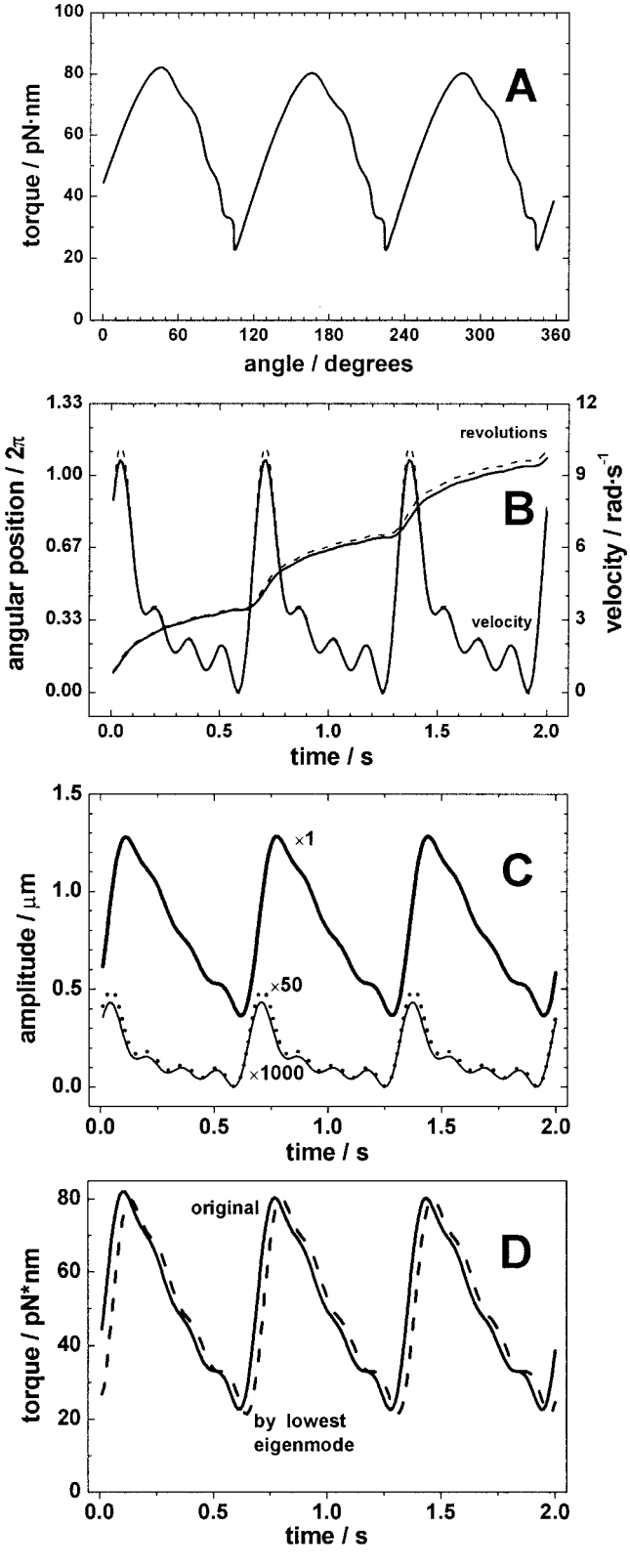

FIGURE 2 Simulation of the viscoelastic deformation of a rotating elastic cantilever that is subjected to a certain torque profile, $\boldsymbol{T}(\theta)$, at its fixed end. (*A*) An assumed torque profile of F_1F_O matching the threefold angular symmetry of ATP hydrolysis in F_1. (*B*) The calculated angular position at the rotation axis in units of 2π, $\theta(t)$, and the angular velocity of the free end, $\boldsymbol{V}(t)$, as function of time. The exact and approximate solutions are shown by the solid and broken curves, respectively (see text for details). (*C*) Time-dependence of the extents of the first tree normal modes $A_0(t)$, $A_1(t)$, and $A_2(t)$ (shown by the *thick solid*, *dashed*, and *thin lines*, respectively). For illustrative purposes the contributions of the first and second "overtones," which are very small, were upscaled by factors of 50 and 1000, respectively. It is obvious that the amplitude of the higher normal modes does, and that of the fundamental mode does not, reproduce the angular velocity profile. (*D*) A comparison of the time courses of the torque (*solid line*) and of the amplitude of the lowest normal mode $A_0(t)$ (*dashed line*). The amplitude of the fundamental mode reproduces the torque profile quite accurately, except for a minor phase shift.

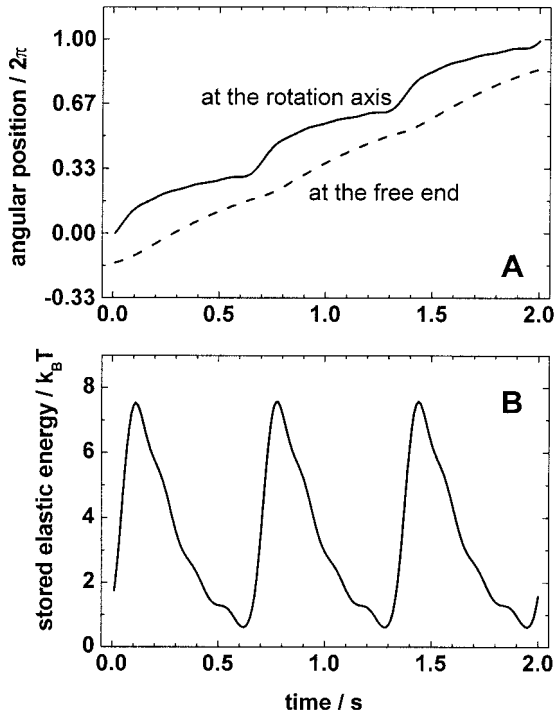

FIGURE 3 Viscoelastic damping of and energy storage by the rotating actin filament. (*A*) Comparison of the angular position of the cantilever as a function of time at the rotation axis (*upper curve*) and at the free end (*lower curve*). (*B*) Elastic energy stored by the cantilever during the nonuniform rotation in units of k_BT (note that the standard ΔG° of ATP hydrolysis, -30 kJ/mol, amounts to $-12.5\ k_BT$).

It was obvious that the higher modes, due to their higher relaxation rate, followed the angular velocity of the rotary enzyme without much delay; however, their extents were negligible. In contrast, the dynamic behavior of the lowest, slowest, and dominating mode was smoothed and phase-shifted.

In Fig. 2 *D* we compared the time course of the torque generated by the enzyme, $\boldsymbol{T}(t)$, and the time-dependence of the extent of the lowest and slowest normal mode, $A_0(t)$. It is obvious that A_0 follows the enzyme's torque quite perfectly, rather than its angular velocity. This insight is further illustrated in Fig. 3. Its upper portion, Fig. 3 *A*, shows the

filament's angular progression at the axis and at the free end, respectively. The average velocity is the same in both cases. The average velocity is proportional to the average torque of the enzyme as assumed in previous work (Noji et al., 1997). The momentary velocities, however, differ between the fixed and the free end. The momentary velocity at the free end reproduces the momentary torque $\boldsymbol{T}(t)$ quite accurately (not shown) but not the momentary velocity of the enzyme, whereas the velocity at the fixed end, by definition, follows the momentary angular velocity of the driving enzyme.

The preceding section has demonstrated the following. The momentary torque generated by the enzyme, or the torque as function of the angular position of the enzyme, can be adequately recorded by a long actin filament that operates against viscous load provided that the viscoelastic relaxation time, $\tau = 1/k_0$ (see Eq. 18), is comparable or longer than the characteristic period of the rotation. Under these conditions, the filament smoothes and phase-shifts the forced rotation ("viscoelastic damping and delay"). The unperturbed transient velocity of the system is, in principle, detectable either by normal modes of the 3-μm-long filament with much shorter relaxation times, being impractical because of their far-too-low amplitudes, or by the basal mode of stiffer and/or shorter filaments. The torque of the enzyme can be monitored by the dominating "slow mode" of the long filament in either of two ways: 1) by the curvature at the axis, or 2) by the momentary angular velocity at the free end. As demonstrated in the previous section, the latter is not as reliable as the former because the motion may be totally obstructed by obstacles, whereas the curvature at the axis does not depend on the physical nature of the counter-torque.

Transient storage of elastic energy by the deformed acting filament

Any deformation of a cantilever can be represented as a sum of its normal modes,

$$y(x, t) = \sum_{n=0}^{\infty} A_n(t) \cdot \tilde{y}_n(x).$$

The elastic energy of the deformation is

$$U_{elast} = \frac{EI}{2} \int_0^L \left(\frac{\partial^2 y}{\partial x^2} \right)^2 dx = \frac{EI}{2} \int_0^L \left(\sum_n A_n \frac{\partial^2 \tilde{y}_n}{\partial x^2} \right)^2 dx$$

$$= \frac{EI}{2} \sum_n \sum_{n'} A_n A_{n'} \int_0^L \frac{\partial^2 \tilde{y}_n}{\partial x^2} \frac{\partial^2 \tilde{y}_{n'}}{\partial x^2} dx \qquad (28)$$

By using the boundary conditions 6 and 14, the latter expression can be integrated:

$$U_{elast} = \frac{EI}{2} \sum_n \sum_{n'} A_n A_{n'} \int_0^L \frac{\partial^4 \tilde{y}_n}{\partial x^4} \tilde{y}_{n'} dx$$

$$= \frac{EI}{2L^4} \sum_n \sum_{n'} A_n A_{n'} \delta_n^4 \int_0^L \tilde{y}_n \tilde{y}_{n'} dx = \frac{EI}{2L} \sum_n \delta_n^4 A_n^2 \qquad (29)$$

When the motion of the cantilever is forced by the torque $\boldsymbol{T}(\theta)$, the coefficients $A_n(t)$ are defined by Eq. 24, and the elastic energy is

$$U_{elast} = \frac{EI}{2L} \sum_n \delta_n^4 \left[b_n \int_0^t a(\tau) \cdot (1 - \exp(k_n(\tau - t))) d\tau \right]^2 \qquad (30)$$

Comparing Eq. 30 with 25 and neglecting the contributions of higher normal modes, we found:

$$U_{elast} = \frac{L}{8EI} \boldsymbol{T}^2 \qquad (31)$$

Thus, the elastic energy stored by the filament is proportional to the length, the square of the torque, and it is reciprocal to the flexural rigidity.

The elastic energy stored by the filament in the course of motion in Fig. 2 *B* was calculated by Eq. 30 and plotted in units of k_BT in Fig. 3 *B*. The elastic energy varied between one and six k_BT units. Considering the average torque generated by the active F-ATPase during the hydrolysis of one molecule of ATP per turn of 120°, namely 20–25 k_BT (Yasuda et al., 1998; Kinosita et al., 1998), the elastically stored energy amounts up to one-fourth of the free energy provided by the cleavage of one molecule of ATP.

Stochastic dynamics of cantilever due to thermal impact (Langevin force)

In the forgoing sections the Brownian motion of the actin cantilever has been neglected. In this section we focus on its fluctuations. The impact of thermal collisions with solvent molecules causes a transient deformation of the cantilever. The elastic energy of the deformation stored between the fixed and free ends of the filament is given by Eq. 29. Thus, the normal modes are independent harmonic oscillators whose dynamics are determined by the stochastic Langevin equations:

$$\frac{dA_n}{dt} + k_n A_n = \sqrt{\frac{2k_BT}{3\Gamma}} \boldsymbol{F}(t) \qquad (32)$$

where k_n denotes the relaxation rate constant as in Eq. 18, Γ is the viscous friction coefficient for the rotating rod of length L, and the random force $\boldsymbol{F}(t)$ satisfies the conditions

$$\langle \boldsymbol{F}_A(t)\rangle = 0, \quad \langle \boldsymbol{F}_A(t_1)\boldsymbol{F}_A(t_2)\rangle = \delta(t_1 - t_2).$$

According to the general theory of the Langevin equation, the time correlation of the coordinate A_n can be calculated by the formula (see, e.g., (Klimontovich, 1986)):

$$\langle A_n(t_1)A_n(t_2)\rangle = \frac{2k_BT}{3\pi\Gamma}\int_0^\infty \frac{\cos(k(t_1 - t_2))}{k_n^2 + k^2}\,dk \qquad (33)$$

In the thermodynamic equilibrium the amplitudes A_n obey the Boltzmann distribution:

$$\rho_n(A_n) = \exp\left(-\frac{EI\delta_n^4 A_n^2}{2Lk_BT}\right) \qquad (34)$$

The flexural rigidity of unconstrained actin filaments and microtubules, EI, has been determined from the amplitude of their thermal bending fluctuations (see Yanagida et al., 1984; Gittes et al., 1993; Isambert et al., 1995). Equation 34 can be used for the analogous analysis of fixed filaments with a fluctuating free end (see the companion paper Pänke et al., 2001). It is noteworthy that the eventual figure of the flexural rigidity is independent of the viscosity of the medium, and even independent of friction of the long filament at the surface of the solid support. It is sensitive, however, to elastic contacts with the surface. They are equivalent to an additional, possibly nonlinear force-field acting on the cantilever, a complication that has not been considered in this work.

Langevin analysis of the forced viscoelastic rotary dynamics

The Brownian thermal forces did not enter in Eq. 27 for the forced rotary dynamics, but they could be introduced by the Langevin stochastic approach. If the angular variation of the torque is small (see Pänke et al., 2001) the Langevin equation can be written as:

$$\Gamma\cdot\dot{\theta} - \boldsymbol{T}(\theta) = \sqrt{2\Gamma k_BT}\cdot\boldsymbol{F}(t) \qquad (35)$$

The extent of the lowest eigenmode, A_0, obeys the stochastic equation

$$\dot{A}_0 + k_0A_0 + \frac{\delta_0^2\boldsymbol{T}(\theta)}{6\Gamma} = \sqrt{2k_BT/3\Gamma}\cdot\boldsymbol{F}(t) \qquad (36)$$

The solution of Eqs. 35 and 36 is represented by two stochastic variables $\theta(t)$ and $A_0(t)$. The mean angular velocity $\bar{\boldsymbol{V}}(\theta)$ can be directly found from Eq. 35 by averaging $\bar{\boldsymbol{V}}(\theta) = \Gamma^{-1}\boldsymbol{T}(\theta)$. If the rate of filament relaxation ω_0 is greater than $\bar{\boldsymbol{V}}$ (that is true in the cases of rotating F-actin filaments), the average deflection $\bar{A}_0$ reads:

$$\bar{A}_0 = -\frac{L\boldsymbol{T}}{2\delta_0^2 EI} \qquad (37)$$

It is noteworthy that the viscosity η does not enter into this equation. This is a consequence of the quasi-equilibrium between the filament and the bulk solution. Instead, the deflection of the filament is entirely determined by the torque $\boldsymbol{T}$ and the flexural rigidity of the filament EI. For a given torque, the amplitude A_0 obeys the Boltzmann statistical distribution:

$$\rho(A_0) = \exp\left(-\frac{EI\delta_0^4(A_0 - \bar{A}_0)^2}{2Lk_BT}\right) \qquad (38)$$

To calculate the autocorrelation of $\theta(t)$ and $A_0(t)$, we introduced new variables $\xi(t) = \boldsymbol{V}(t) - \bar{\boldsymbol{V}}$, $\zeta(t) = A_0(t) - \bar{A}_0$, and expanded them under the Fourier integrals:

$$\xi(t) = \frac{1}{2\pi}\int_{-\infty}^{\infty}\xi_\omega e^{-i\omega t}d\omega \quad \text{and} \quad \zeta(t) = \frac{1}{2\pi}\int_{-\infty}^{\infty}\zeta_\omega e^{-i\omega t}d\omega$$

Substituting these variables into 35 and 36, we obtained two algebraic equations for the Fourier components ξ_ω and ζ_ω:

$$\Gamma\cdot\xi_\omega = \sqrt{2\Gamma k_BT}\cdot\boldsymbol{F}_\omega \qquad (39a)$$

and

$$(-i\omega + \omega_0)\cdot\zeta_\omega = \sqrt{2k_BT/3\Gamma}\cdot\boldsymbol{F}_\omega \qquad (39b)$$

where $\boldsymbol{F}_\omega$ is the Fourier transform of the Langevin source $F(t)$. The autocorrelation functions $\langle\xi\xi\rangle_t$ and $\langle\zeta\zeta\rangle_t$ are connected with the spectral densities $(\xi\xi)_\omega$ and $(\zeta\zeta)_\omega$ by the Fourier transformation, $\langle\xi\xi\rangle_t = \frac{1}{2\pi}\int_{-\infty}^{\infty}(\xi\xi)_\omega e^{i\omega t}d\omega$, $\langle\zeta\zeta\rangle_t = \frac{1}{2\pi}\int_{-\infty}^{\infty}(\zeta\zeta)_\omega e^{i\omega t}d\omega$. The functions $(\xi\xi)_\omega$ and $(\zeta\zeta)_\omega$ are connected with ξ_ω and ζ_ω (see, e.g., Klimontovich, 1986), yielding the following spectral densities

$$(\xi\xi)_\omega = \frac{2k_BT}{\Gamma} \quad \text{and} \quad (\zeta\zeta)_\omega = \frac{2k_BT}{3\Gamma(\omega^2 + \omega_0^2)} \qquad (40a,b)$$

and the autocorrelation functions:

$$\langle\xi\xi\rangle_t = \frac{k_BT}{\Gamma}\,\delta(t) \quad \text{and} \quad \langle\zeta\zeta\rangle_t = \frac{k_BT}{3\pi\Gamma}\int_{-\infty}^{\infty}\frac{\cos(\omega t)}{\omega^2 + \omega_0^2}\,d\omega \qquad (41a,b)$$

Equations 37 and 38 are particularly useful for the analysis of rotation experiments aiming at a determination of both 1) the flexural rigidity of the filament as a probe and 2) the torque of the rotary enzyme to which the filament is attached. This technique was applied to the rotary F_OF_1-ATPase as detailed in the companion paper (Pänke et al., 2001).

SUMMARY AND CONCLUSIONS

This article describes the static, dynamic, and stochastic behavior of actin cantilevers that are connected to the rotor portion of ATP synthase when its stator is fixed to a solid support. The study aims at the detailed rotary characteristics of this enzyme. The actin filament, approximated as a cylindrical rod with a typical radius $R = 2.8$ nm and length $L = 1$–3 μm, was treated as a continuous medium. Its elastic behavior was assumed to be Newtonian, and it was characterized by a single parameter, *EI*, the *flexural rigidity*. For actin filaments *EI* is typically $\sim 10^{-25}$ N · m^2 (Gittes et al., 1993; Yasuda et al., 1996). Our approach was based on the linear theory of elasticity; it was limited to small deformations. The viscoelastic normal modes of the actin cantilever were calculated under the assumption of motion in a homogeneous viscous medium.

The lowest dynamic mode ($n = 0$) broadly resembles a statically bent cantilever with a concentrated load acting on its very end, as known from the macroscopic world. The overtones have $n = 1, 2, \ldots$ nodes over the full length. The characteristic relaxation times are quite different, they scale by $\eta L^4/EI$ and are modulated by δ_n^{-4}, wherein δ_n denotes a characteristic factor for each normal mode which is geometry- and medium-independent. Because of the dependence on the fourth power of the parameter δ_n (which progresses as $\sim$1.9, 4.7, 7.9, 11, ... starting from $n = 0$) the relaxation time of the second mode is 37 times shorter than of the first mode, the one of the third 299 times, and of the fourth 1123 times shorter. For a given filament of full length 3 μm the ground mode relaxes in 150 ms, that is, 40 times slower than the relaxation of an unconstrained filament with the similar length.

When the enzyme turns over it creates torque and rotates the actin filament. Counter-torque is generated by viscous drag in the medium. If accelerating pulses of the driving rotary motion occur in the typical time range of some ten milliseconds, the higher bending modes follow with little delay, but not the ground mode. Its relaxation is simply too slow. The higher modes, however, are of such a small amplitude that the slow response of the ground mode dominates the experimentally accessible behavior. Therefore, the *observable* motion of the filament is smoothed and phase-shifted relative to the driving rotation of the enzyme ("visco-elastic damping and delay"). What appears as a deficit at the first sight is advantageous at closer inspection. The extent of the ground mode as function of the angular position of the filament reflects the torque as a function of the angular position of the filament. The torque is apparent both from the curvature of the filament at its "fixed" end and from the angular velocity at the free end. The curvature is a more reliable indicator than the velocity because an obstacle on the surface of the solid support may totally block the angular progression despite persisting torque, whereas the cantilever will still be bent. Unfortunately, the inherently limited optical resolution prevents accurate measurement of the curvature at the very axis of rotation. Taking a filament of 3-μm length one can only "see" the overall curvature over the last 0.5–3 μm of the total length. At any given torque of the enzyme, however, the overall curvature of the actin cantilever differs depending on the particular force distribution over length, whether it is linear by viscous drag (rotating filament), constant by surface friction, or concentrated by an obstacle (blocked filament). In this article we showed that the *invisible* curvature at the axis can be extrapolated with fair precision from the *visible* curvature along the few micrometer length of the filament. This extrapolation yields the enzyme's torque rather independently of whether the major counter-force results from the viscous drag, the surface-friction, or a surface obstacle. In the companion paper (Pänke et al., 2001) this insight is applied to evaluate the angular dependence of the enzyme's torque as function of the angular reaction coordinate.

In previous works the average torque has been inferred from the detected average rate of rotation of actin filaments (Yasuda et al., 1998; Omote et al., 1999; Pänke et al., 2000). The calculated figures have been based on the assumption that the filament rotates in a homogeneous medium with the viscosity of water ($\sim 10^{-3}$ kg^{-1} s^{-1}). This assumption is questionable for two obvious complications; 1) the medium viscosity very close to the surface can be much larger than in the bulk (Hunt et al., 1994) and 2) elastic and inelastic contacts with the surface may slow or even totally block the rotation. This is why we favor studying the curvature of actin filaments to evaluate the torque. In this case the calibration has to rely on the flexural rigidity of the actin filament. It can be determined from the amplitude of bending fluctuations, either of fixed actin filaments by Eq. 34 or of the same rotating filament by Eq. 38. It is noteworthy that the eventual figure of the flexural rigidity is independent of the viscosity of the medium, and even independent of friction (inelastic contacts) at the surface of the solid support.

The analysis of the curvature of actin filaments allows us to more precisely estimate the magnitude of the torque and the torque profile over the angular reaction coordinate. The application of these considerations to data on the rotation of subunit γ in the isolated F_1 portion and on the rotation of the **c**-ring in F_OF_1 is the subject of the companion paper.

APPENDIX

Nonlinear Deformation of an Elastic Cantilever

According to the nonlinear theory of elasticity (Landau and Lifshitz, 1959), the deformation $y(x)$ of an elastic cantilever with the length L and the flexural rigidity EI as caused by an orthogonal concentrated force $\boldsymbol{F}$ can be expressed parametrically through the elliptic integral

$$y(\theta) = \sqrt{\frac{EI}{2\boldsymbol{F}}} \cdot \int_{\theta}^{\pi/2} \frac{\cos(\zeta)}{\sqrt{\cos(\xi) - \cos(\zeta)}}\, d\zeta \qquad \text{(A1)}$$

$$x(\theta) = \sqrt{2EI/\boldsymbol{F}} \cdot \left(\sqrt{\cos(\xi)} - \sqrt{\cos(\xi) - \cos(\theta)}\right) \qquad \text{(A2)}$$

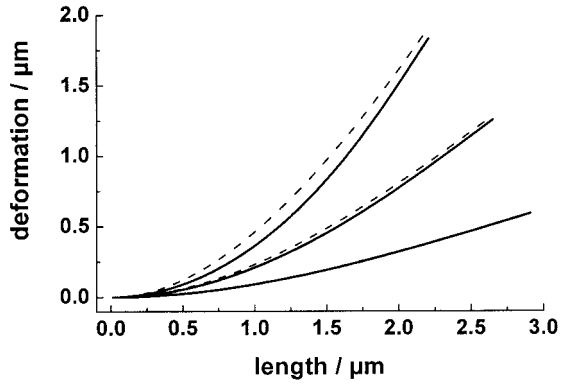

FIGURE 4 Static deformation of an elastic cantilever with length $3 \cdot 10^{-6}$ m and flexural rigidity 10^{-25} N · m^2 calculated by Eqs. A1–A3 (the nonlinear theory, *solid lines*) and by Eq. 9 (the linear approximation, *dashed lines*). The lower, middle, and upper pairs of curves were calculated for the torque values of 20, 50, and 100 pN · nm, respectively (concentrated counterforce applied at the end).

where the parameter ξ is the solution of an integral equation

$$L = \sqrt{\frac{EI}{2F}} \cdot \int_{\xi}^{\pi/2} \frac{d\zeta}{\sqrt{\cos(\xi) - \cos(\zeta)}} \qquad \text{(A3)}$$

We compared the numerical solution of equations A1–A3 with the linear Eq. 9 using the same parameters as in Fig. 1 ($L = 3 \cdot 10^{-6}$ m, $EI = 10^{-25}$ N · m^2). The nonlinear solutions are shown in Fig. 4 by solid lines, the linear are plotted by dashed lines. The lower, middle, and upper pairs of curves were calculated for the torque values of 20, 50, and 100 pN · nm, respectively. These data show that the linear theory of elasticity is approximately valid even at a very high torque of 100 pN · nm.

We express our thanks to our colleagues Drs. Oliver Pänke and Siegfried Engelbrecht for fruitful discussion and collaboration, and to Prof. Peter Hertel (Physics Department, Osnabrück) for advice and encouragement during the early stages.

This work was financially supported by the Alexander von Humboldt Foundation (to D.C.) and by Deutsche Forschungsgemeinschaft Grant SFB 431-D1 and the Human Science Frontier Program (to W.J.) (Grant RG15-1998-M).

REFERENCES

Abrahams, J. P., A. G. W. Leslie, R. Lutter, and J. E. Walker. 1994. The structure of F_1-ATPase from bovine heart mitochondria determined at 2.8 Å resolution. *Nature.* 370:621–628.

Adachi, K., R. Yasuda, H. Noji, H. Itoh, Y. Harada, M. Yoshida, and K. Kinosita, Jr. 2000. Stepping rotation of F1-ATPase visualized through angle-resolved single-fluorophore imaging. *Proc. Natl. Acad. Sci. U.S.A.* 97:7243–7247.

Berg, H. C. 1993. Random Walks in Biology. Princeton University Press, Princeton, New Jersey.

Beth, R. A. 1967. Statics of elastic bodies. *In* Handbook of Physics. E. U. Condon and H. Odishaw, editors. McGraw-Hill Book Company, New York.

Boyer, P. D. 1997. The ATP synthase: a splendid molecular machine. *Annu. Rev. Biochem.* 66:717–749.

Cherepanov, D. A., A. Mulkidjanian, and W. Junge. 1999. Transient accumulation of elastic energy in proton translocating ATP synthase. *FEBS Lett.* 449:1–6.

Courant, R., and D. Hilbert. 1962. Methods of Mathematical Physics. Wiley, New York.

Duncan, T. M., Y. Zhou, V. V. Bulygin, M. L. Hutcheon, and R. L. Cross. 1995. Probing interactions of the *Escherichia coli* F_0F_1 ATP synthase β and gamma subunits with disulphide cross-links. *Biochem. Soc. Trans.* 23:736–741.

Gittes, F., B. Mickey, J. Nettleton, and J. Howard. 1993. Flexural rigidity of microtubules and actin filaments measured from thermal fluctuations in shape. *J. Cell Biol.* 120:923–934.

Happel, J., and H. Brenner. 1983. Low Reynolds number hydrodynamics. Martinus Nijhoff Publishers, the Hague.

Häsler, K., S. Engelbrecht, and W. Junge. 1998. Three-stepped rotation of subunits γ and ϵ in single molecules of F-ATPase as revealed by polarized, confocal fluorometry. *FEBS Lett.* 426:301–304.

Hunt, A. J., F. Gittes, and J. Howard. 1994. The force exerted by a single kinesin molecule against a viscous load. *Biophys. J.* 67:766–781.

Isambert, H., P. Venier, A. C. Maggs, A. Fattoum, R. Kassab, D. Pantaloni, and M. F. Carlier. 1995. Flexibility of actin filaments derived from thermal fluctuations. Effect of bound nucleotide, phalloidin, and muscle regulatory proteins. *J. Biol. Chem.* 270: 11437–11444.

Jones, P. C., and R. H. Fillingame. 1998. Genetic fusions of subunit c in the F_0 sector of H^+-transporting ATP synthase: functional dimers and trimers and determination of stoichiometry by cross-linking analysis. *J. Biol. Chem.* 273:29701–29705.

Junge, W., H. Lill, and S. Engelbrecht. 1997. ATP synthase: an electrochemical transducer with rotatory mechanics. *TIBS.* 22:420–423.

Kinosita, K., R. Yasuda, H. Noji, S. Ishiwata, and M. Yoshida. 1998. F_1-ATPase: a rotary motor made of a single molecule. *Cell.* 93: 21–24.

Klimontovich, Yu. L. 1986. Statistical Physics. Gordon and Breach, Harwood Academic Publishers, New York.

Landau, L., and E. M. Lifshitz. 1959. Theory of Elasticity. Pergamon Press, London.

Leslie, A. G., J. P. Abrahams, K. Braig, R. Lutter, R. I. Menz, G. L. Orriss, M. J. van Raaij, and J. E. Walker. 1999. The structure of bovine mitochondrial F_1-ATPase: an example of rotary catalysis. *Biochem. Soc. Trans.* 27:37–42.

Mendelson, R., and E. P. Morris. 1997. The structure of the acto-myosin subfragment 1 complex: results of searches using data from electron microscopy and x-ray crystallography. *Proc. Natl. Acad. Sci. U.S.A.* 94:8533–8538.

Noji, H., R. Yasuda, M. Yoshida, and K. Kinosita. 1997. Direct observation of the rotation of F-ATPase. *Nature.* 386:299–302.

Omote, H., N. Samborunatsu, K. Saito, Y. Sambongi, A. Iwamoto-Kihara, T. Yanagida, Y. Wada, and M. Futai. 1999. The γ subunit rotation and torque generation in F_1-ATPase from wild-type or uncoupled mutant *Escherichia coli. Proc. Natl. Acad. Sci. U.S.A.* 96:7780–7784.

Oster, G., and H. Wang. 1999. ATP synthase: two motors, two fuels. *Structure.* 7:R67–R72.

Pänke, O., D. A. Cherepanov, K. Gumbiowski, S. Engelbrecht, and W. Junge. 2001. Viscoelastic dynamics of actin filaments coupled to rotary F-ATPase: angular torque profile of the enzyme. *Biophys. J.* 81:1220–1233.

Pänke, O., K. Gumbiowski, W. Junge, and S. Engelbrecht. 2000. F-ATPase: specific observation of the rotating c-subunit oligomer of EF_OEF_1. *FEBS Lett.* 472:34–38.

Pänke, O., and B. Rumberg. 1999. Kinetic modeling of rotary CF_0F_1-ATP synthase: storage of elastic energy during energy transduction. *Biochim. Biophys. Acta.* 1412:118–128.

Sabbert, D., S. Engelbrecht, and W. Junge. 1996. Intersubunit rotation in active F-ATPase. *Nature.* 381:623–626.

Sabbert, D., S. Engelbrecht, and W. Junge. 1997. Functional and idling rotatory motion within F-ATPase. *Proc. Natl. Acad. Sci. U.S.A.* 94: 4401–4405.

Sabbert, D., and W. Junge. 1997. Stepped versus continuous rotatory motors at the molecular scale. *Proc. Natl. Acad. Sci. U.S.A.* 94: 2312–2317.

Sambongi, Y., Y. Iko, M. Tanabe, H. Omote, A. Iwamoto-Kihara, I. Ueda, T. Yanagida, Y. Wada, and M. Futai. 1999. Mechanical rotation of the c subunit oligomer in ATP synthase (F_OF_1): direct observation. *Science.* 286:1722–1724.

Seelert, H., A. Poetsch, N. A. Dencher, A. Engel, H. Stahlberg, and D. J. Mueller. 2000. Proton-powered turbine of a plant motor. *Nature.* 405: 418–419.

Stock, D., A. G. Leslie, and J. E. Walker. 1999. Molecular architecture of the rotary motor in ATP synthase. *Science.* 286:1700–1705.

Tsunoda, S. P., R. Aggeler, H. Noji, K. Kinosita, M. Yoshida, and R. A. Capaldi. 2000. Observations of rotation within the F_OF_1-ATP synthase: deciding between rotation of the F(o)c subunit ring and artifact. *FEBS Lett.* 470:244–248.

Yanagida, T., M. Nakase, K. Nishiyama, and F. Oosawa. 1984. Direct observation of motion of single F-actin filaments in the presence of myosin. *Nature.* 307:58–60.

Yasuda, R., H. Miyata, and K. Kinosita, Jr. 1996. Direct measurement of the torsional rigidity of single actin filaments. *J. Mol. Biol.* 263:227–236.

Yasuda, R., H. Noji, K. Kinosita, and M. Yoshida. 1998. F_1-ATPase is a highly efficient molecular motor that rotates with discrete 120° steps. *Cell.* 93:1117–1124.